ORIGINAL RESEARCH ARTICLE

Carbothermic Reduction of Zinc Containing Industrial Wastes: A Kinetic Model

M. LEUCHTENMUELLER, C. LEGERER, U. BRANDNER, and J. ANTREKOWITSCH

Effective recycling of zinc-containing industrial wastes, most importantly electric arc furnace dust, is of tremendous importance for the circular economy of the steel and zinc industry. Herein, we propose a comprehensive kinetic model of the combined carbothermic and metallothermic reduction of zinc oxide in a metal bath process. Pyro-metallurgical, large-scale lab experiments of a carbon-saturated iron melt as reduction agent for a molten zinc oxide slag were performed to determine reaction constants and accurately predict mass transfer coefficients of the proposed kinetic model. An experimentally determined kinetic model demonstrates that various reactions run simultaneously during the reduction of zinc oxide and iron oxide. For the investigated slag composition, the temperature-dependent contribution of the metallothermic zinc oxide reduction was between 25 and 50 pct of the overall reaction mechanism. The mass transfer coefficient of the zinc oxide reduction quadrupled from 1400 °C to 1500 °C. The zinc recovery rate was > 99.9 pct in all experiments.

https://doi.org/10.1007/s11663-020-02047-9

I. INTRODUCTION

ZINC (Zn) is the fourth most produced metal worldwide (13 million tons per year) following iron, aluminum and copper. The applications of zinc range from predominately galvanizing steel, over brass alloy products, to super pure zinc oxide.[1] Despite its widespread use, Zn has a rare abundance of only 70 ppm in the earth's crust (*e.g.* abundance of Fe 5.63 pct and Al 8.23 pct), which emphasis the importance of a resource-conserving usage focused on the mitigation of production and recycling losses.[2] Yet, the global end-of-life recycling rate of Zn is a mere 33 pct, where the largest part of Zn losses occur during waste management, causing excessive, potentially hazardous Zn emissions.[3] In addition, low efficiencies of existing recycling technologies further exacerbate the low Zn recycling rate, and highlight the tremendous need to improve Zn-containing industrial waste recycling processes.[4–7]

Main Zn-containing industrial wastes are leaching residues and jarosite from primary zinc production, lead slags and electric arc furnace dust (EAFD).[6,8–10] EAFD is a waste material of steel recycling that contains up to 43 pct of Zn.[11] In steel recycling, scrap steel is melted at high temperatures in an electric arc furnace (EAF). During this process volatile elements including Zn from galvanized steel scrap evaporate and ultimately accumulate as EAFD. Other elements present in EAFD are Fe, Pb, Cd, Na, K, halides and slag building compounds such as CaO and SiO_2.[12] In 2018, the global steel production was 1807 million tons (MT), 520 MT of which were produced *via* the EAF route.[13] Per ton of liquid EAF steel[14–16] 10 to 25 kg of EAFD are typically generated (depending on scrap composition and furnace operation,[12,17]) which sum to approximately a yearly EAFD generation of 5.2 to 13 MT.[18] Moreover, the EAF steel production is forecasted to increase up to 1000 MT in 2050, in which case the annual dust generation could increase up to 25 MT.[19] Given such substantial quantities and the high average Zn-content, EAFD is a considerable secondary resource of valuable Zn.

Despite the high Zn content, less than 50 pct of the generated EAFD is recycled globally,[18] and in most developed countries EAFD is classified as hazardous waste (US EPA: K061,[20] European Waste Catalogue (EWC) 10 02 07*[21] and Ministry of Environment in Canada 143H[22]), due to its high heavy metal concentrations. Environmental regulations in the US, EU and Canada therefore require stabilization treatment, before EAFD can be landfilled, which contributes significantly

M. LEUCHTENMUELLER, U. BRANDNER, and J. ANTREKOWITSCH are with the Chair of Non-Ferrous Metallurgy, Montanuniversität Leoben, Franz-Josef-Strasse 18, 8700 Leoben, Austria. Contact e-mail: manuel.leuchtenmueller@unileoben.ac.at C. LEGERER is with the Rural Clinical School, Faculty of Medicine, University of New South Wales, Sydney, NSW 2052, Australia.

Manuscript submitted May 5, 2020; accepted December 3, 2020. Article published online January 6, 2021.

to the EAFD disposal costs. The high specific volume and concomitant low bulk density (1.1 to 2.5 g/cm^3) of EAFD further contribute to the ecologic impact and land filling related costs of EAFD.[6] As a result, EAFD is predominantly recycled in jurisdictions where environmental policies demand low leachability and prohibit cost-efficient landfilling. The most successful recycling processes for EAFD are based on a carbothermic high–temperature reduction reaction.

II. CARBOTHERMIC EAFD RECYCLING PROCESSES

The fundamental chemical principle of zinc recovery from EAFD is identical in all industrial pyro-metallurgical processes: ZnO is carbothermically reduced to Zn, which then volatilizes into the gas phase. After leaving the reaction zone gaseous Zn is typically combusted to ZnO, which is subsequently captured in bag house filters. The main impurities of the obtained crude zinc oxide (CZO) are other volatile elements originating in EAFD: Pb, Cd, K, Na, Cl, F. In a final processing step the CZO is washed to remove chlorides and ultimately used as a secondary resource in the primary zinc industry.

Currently available EAFD recycling processes can be classified according to the physical state of the reactants, ZnO and C. In the most commonly used Waelz kiln, RHF and MHF, the pyro-chemical reaction is a solid–solid reduction between carbon and ZnO or a solid–gaseous reaction between CO and ZnO.[23,24] Other furnaces to treat EAFD are the electric arc, plasma and induction furnace, in which the reduction reaction is of (1) the solid–liquid type between coke and ZnO dissolved in a molten slag phase or of (2) the liquid–liquid type between dissolved carbon in the metal and ZnO in the slag.[25–27]

These underlying reaction types have a critical impact on the performance of EAFD recycling methods. Processes based on solid–solid reactions demonstrate relatively low Zn recovery rates, slow reaction kinetics which require large kiln dimensions (incurring high capital costs and heat losses), and generate a slag that is commonly landfilled. In comparison, processes with underlying liquid-liquid reaction mechanisms are usually performed at elevated temperatures showing faster reaction kinetics, lower capital costs and improved economic flexibility due to the production of a marketable slag phase as an additional production.[28] But these processes are more energy intensive and exhibit increased refractory wear and therefore operating costs. Consequently, the lower overall energy consumption of the solid–solid reaction in connection with the counter-current operation mode are the decisive determinants for the uncontested success of the Waelz kiln process to recycle EAFD to date. Nonetheless, the Waelz kiln as the current state-of-the-art processes is far from optimal. For example, the Waelz kiln only demonstrates Zn recovery rates of roughly 85 pct, leaving room for progress. Table I lists process parameters for a typical Waelz kiln.

A significant amount of research has been conducted to find alternative concepts to the described C-based high-temperature EAFD recycling process. Investigated approaches range from Zn volatilization with halogenation[34] over hydrometallurgical approaches[35,36] to physical separation processes, such as magnetic and air separation[37,38] and combinations of pyro- and hydrometallurgical approaches.[39,40] However, due to the complex morphology of EAFD, these alternatives demonstrated either insufficient recovery rates or industrial viability compared to the state-of-art process.[41,42]

An initial step towards improvement of conventional, carbothermic processes (*e.g.* recovery rates) and development of new solutions require a more detailed understanding of the underlying reaction mechanisms and kinetics. In 1996, Donald and Pickles demonstrated a Zn recovery rate of almost 100 pct for a liquid–liquid concept in which a carbon-saturated iron melt is used as reduction agent to recycle EAFD.[15] The reported reaction mechanism (Eqs. [1] to [3]) describes the high-temperature reduction of ZnO and FeO with dissolved carbon,[43] and the metallothermic reduction of ZnO with liquid Fe.[44]

$$\mathrm{ZnO_{l,slag}} + \mathrm{C_{l,metal}} \rightarrow \mathrm{Zn_{gas}} + \mathrm{CO_{gas}} \quad [1]$$

$$\mathrm{FeO_{l,slag}} + \mathrm{C_{l,metal}} \rightarrow \mathrm{Fe_{l,metal}} + \mathrm{CO_{gas}} \quad [2]$$

$$\mathrm{ZnO_{l,slag}} + \mathrm{Fe_{l,metal}} \rightarrow \mathrm{Zn_{gas}} + \mathrm{FeO_{l,slag}} \quad [3]$$

Kinetic studies mainly exist for the solid–solid reduction of ZnO,[45–48] but the reaction kinetics of the liquid–liquid ZnO reduction is poorly understood. Notably, the contribution of Fe to the overall reduction of ZnO with a C-saturated iron melt remains to be clarified. The goals of this paper, therefore, are twofold: (1) to postulate a comprehensive kinetic model helping to get a better understanding of how the constituents within the metal and slag phase react, and (2) to determine concomitant model parameters based on high-temperature experiments to accurately describe the reaction kinetics of the ZnO and FeO reduction. Finally, we also present mass transfer coefficients for the ZnO and FeO reduction accounting for all experimental assumption to assist the development of industrial EAFD recycling processes.

III. MATERIALS AND METHODS

A. *Source Materials and Experimental Setup*

The reduction mechanism between liquid ZnO and carbon dissolved in liquid Fe was studied in controlled experimental conditions by continuous monitoring of compositions and temperature. A synthetic slag, a C-saturated iron alloy and pure ZnO (> 99 pct) were melted in a graphite crucible (inner-diameter 180 mm, inner-height 270 mm, wall thickness 30 mm) which was heated by an induction furnace (max. power input 80

kW; ITG Induktionsofenanlagen GmbH, Hirschhorn, Germany). Figure 1 illustrates the reaction mechanism and gives an overview of the experimental setup.

Prior to the reduction experiment a carbon-saturated iron master alloy was prepared by adding graphite to S235 construction steel. In a similar way a slag was prepared by remelting pure quartz, lime, and alumina. The ratio between CaO and SiO_2 1.2. To lower the liquidus temperature of the system, Al_2O_3 was added. According to FactSage calculations, the lowest possible liquidus temperature in slag system is reached at around 16 pct Al_2O_3. The final composition of the prepared slag was 38.4 pct SiO_2, 47.5 pct CaO and 14.1 pct Al_2O_3. The detailed procedure for six high-temperature reduction experiments included the following steps:

1. Preheating of the graphite crucible to the desired temperature (1420 °C to 1530 °C)
2. Feeding of the iron master alloy and the synthetic slag mixture
3. Melting and temperature homogenization
4. Feeding of the pure ZnO (> 99 pct)
5. Slag sampling in defined time intervals
6. Temperature reference measurements to calibrate the pyrometer (a minimum of three)
7. Chemical analysis of slag samples

The graphite crucible was covered by a perforated cover (hole diameter 60 mm) to prevent excessive heat losses and achieve a homogenous temperature distribution across the melt. At the bottom of the furnace a pyrometer continually recorded the crucible surface temperature. A custom-made furnace controller (PID algorithm) regulated the furnace power to ensure a constant crucible temperature and therefore isothermal conditions within the crucible. Additionally, three to four temperature measurements per experiment were recorded with commercially available type-S immersion thermocouples (Minkon GmbH, Erkrath, Germany), these measurements were used in the kinetic model.

After cooling to room temperature, the slag samples were ground in a vibration mill, fixed to adhesive tape and analyzed using energy-dispersive X-ray spectroscopy within a scanning electron microscope. The chemical analyses were recalculated and normalized to account for the corresponding oxidic forms (Ca to CaO, Si to SiO_2, Al to Al_2O_3, Zn to ZnO and Fe to FeO) of the measured elements.

The reduction of ZnO from the slag and the Fe oxidation into the slag influence the total slag mass and consequently the chemical analysis. To account for these changes in the kinetic model, effective FeO and ZnO concentrations (Figure 2) are calculated in Eqs. [4] and [5]. The measured FeO and ZnO concentrations are multiplied with the ratio of slag building compounds at the start ($t = 0$) and each sampling time (t). The effective FeO and ZnO concentrations are subsequently denoted as [ZnO] and [FeO].

$$[\mathrm{ZnO}] = \mathrm{Effective\_ZnO}_{(t)} = \mathrm{Measured\_ZnO}_{(t)} \frac{(\mathrm{SiO_2} + \mathrm{Al_2O_3} + \mathrm{CaO})_{t=0}}{(\mathrm{SiO_2} + \mathrm{Al_2O_3} + \mathrm{CaO})_t} \quad [4]$$

$$[\mathrm{FeO}] = \mathrm{Effective\_FeO}_{(t)} = \mathrm{Measured\_FeO}_{(t)} \frac{(\mathrm{SiO_2} + \mathrm{Al_2O_3} + \mathrm{CaO})_{t=0}}{(\mathrm{SiO_2} + \mathrm{Al_2O_3} + \mathrm{CaO})_t} \quad [5]$$

Table I. Typical Process Parameters for Waelz Kilns[24,29–33]

Slag	Length	Diameter	Carbon	CO_2	Zn in Slag
560 to 650 kg	38.5 to 60.0 m	3.0 to 4.2 m	160 to 200 kg/ton EAFD	580 to 730 kg/ton EAFD	~ 5 pct

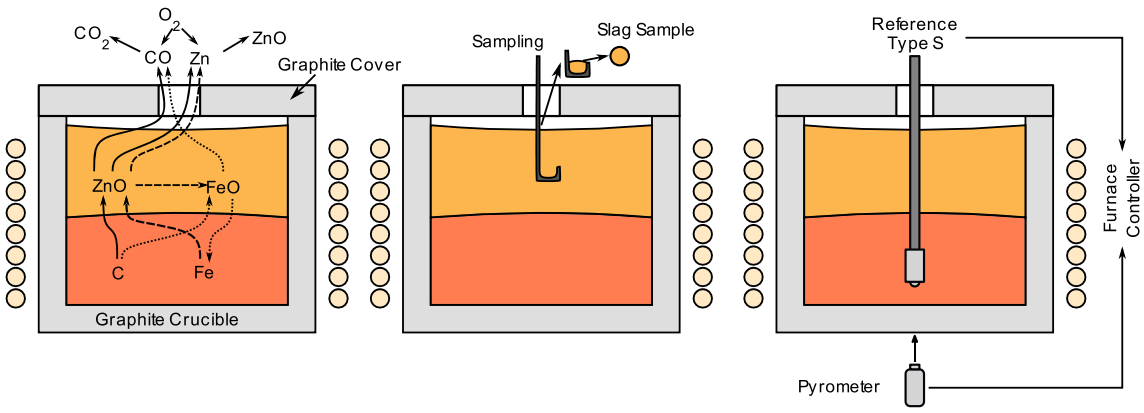

Fig. 1—Overview of the reaction mechanism and experimental setup, sampling procedure and temperature reference measurements.

B. *Kinetic Model*

In physical chemistry, kinetic models describe the effect of chemical kinetics on the rate of a reaction. As such, mathematical models of reaction kinetics are frequently applied to optimize process conditions (*e.g.* temperature and pressure) and product yield in the design or modification of chemical reactors. In the following we present the construction of a mathematical model that describes in detail the characteristics of the reduction reactions between a carbon-saturated iron melt and a synthetic slag system containing ZnO. The presented approach establishes reaction rates for the reaction mechanism (Eqs. [1] to [3]) and combines the resulting partial differential equations to yield a depended system of linear ordinary differential equations (ODE). Obtained isothermal experimental data can be fitted to respective ODEs, yielding rate constants for FeO and ZnO. A combination of these individual rate constant with the Arrhenius equation allows the calculation of temperature dependent rate constants. To account for other process conditions, mass transfer coefficients for both reactants are stated. In summary, this kinetic model expands on the concept of a liquid carbon-saturated iron melt used to recycle Zn-containing waste material (*e.g.* EAFD),[22] which is determined by two carbothermic reactions underpinning the reduction of ZnO and FeO (Eqs. [1] to [2]) and a metallothermic reaction between Fe and ZnO (Eq. [3]).

The net reaction rate of each chemical reactions is defined as the difference between the rate of reaction and reverse reaction (Eq. [6]). When the rate of reaction and reverse reaction are identical, the net reaction rate is zero and the reaction has reached an equilibrium state.

$$\text{Net reaction rate} = \text{Reaction rate} - \text{Reversereactionrate} \quad [6]$$

The net reaction rate for the reduction reaction between liquid FeO and carbon dissolved in liquid metal (shown in Eq. [2]) is described as follows:

$$-\frac{\mathrm{d}[\mathrm{FeO}]}{\mathrm{d}t} = k'_{\mathrm{FeO-C}} \cdot (\mathrm{C}) \cdot [\mathrm{FeO}] - k'_{\mathrm{FeO-oxi}} \cdot (\mathrm{Fe}) \cdot \{\mathrm{CO}\} \quad [7]$$

where $k'_{\mathrm{FeO-C}}$ and $.k'_{\mathrm{FeO-oxi}}$ correspond to the kinetic constants (rate constants) of the reaction and reverse reaction, respectively. The reaction rate is a product of $k'_{\mathrm{FeO-C}}$, the carbon concentration of the metal (C) and the FeO concentration in the slag [FeO]. Conversely, the reverse reaction rate is proportional to $k'_{\mathrm{FeO-oxi}}$, the Fe-concentration in the metal (Fe), the CO partial pressure at the phase boundary {CO}.

The continuous consumption of carbon according to Eqs. [1] and [2] would allow the conclusion of a dropping carbon concentration. However, the reduction process was performed in a graphite crucible, which is why the carbon concentration was assumed to be constant. Similarly, the assumption was made that Fe concentration in the metal bath would remain nearly constant. Additionally, the process slag was held at a stable level resulting in a steady partial pressure of developing CO gas bubbles. These assumptions are considered by the simplified rate constants $k_{\mathrm{FeO-C}}$ and $k_{\mathrm{FeO-Oxi}}$:

$$-\frac{\mathrm{d}[\mathrm{FeO}]}{\mathrm{d}t} = k_{\mathrm{FeO-C}} \cdot [\mathrm{FeO}] - k_{\mathrm{FeO-Oxi}} \quad [8]$$

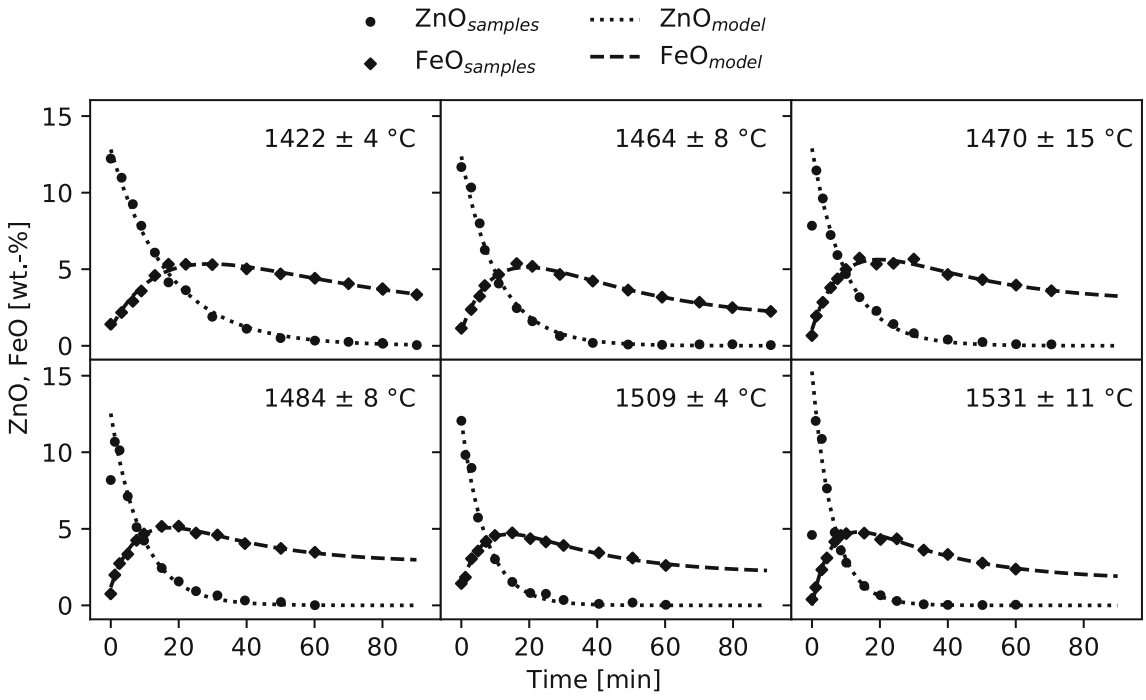

Fig. 2—Measured FeO and ZnO concentrations plotted over time compared to fitted equations for six isothermal experiments at increasing temperatures; insert: average and deviation of temperature measurements (type-S immersion thermocouple).

The same procedure is used to simplify the net reaction rate of the ZnO reduction (Eq. [1]) and the metallothermic reaction between Fe and ZnO (Eq. [3]). In the prior reaction, gaseous Zn leaves the reaction zone during the first stage of the reaction and therefore, allow for the assumption of non–reversibility.[49] Equation [10] highlights that the resulting reaction rates of the metallothermic reaction are linked by the FeO to ZnO molar mass ratio.

$$-\frac{\mathrm{d}[\mathrm{ZnO}]}{\mathrm{d}t} = k_{\mathrm{ZnO-C}} \cdot [\mathrm{ZnO}] \qquad [9]$$

$$-\frac{\mathrm{d}[\mathrm{ZnO}]}{\mathrm{d}t} = \frac{\mathrm{d}[\mathrm{FeO}]}{\mathrm{d}t} \cdot \frac{M_{\mathrm{FeO}}}{M_{\mathrm{ZnO}}} = k_{\mathrm{ZnO-Fe}} \cdot [\mathrm{ZnO}] \qquad [10]$$

Subsequently, the combined reaction rates of FeO and ZnO, which describe the interdependence between all three reduction reactions (Eqs. [1] to [3]) is derived:

$$-\frac{\mathrm{d}[\mathrm{FeO}]}{\mathrm{d}t} = k_{\mathrm{FeO-C}} \cdot [\mathrm{FeO}] - k_{\mathrm{Fe-Oxi}} - k_{\mathrm{ZnO-Fe}} \cdot [\mathrm{ZnO}] \cdot \frac{M_{\mathrm{ZnO}}}{M_{\mathrm{FeO}}} \qquad [11]$$

$$-\frac{\mathrm{d}[\mathrm{ZnO}]}{\mathrm{d}t} = k_{\mathrm{ZnO-C}} \cdot [\mathrm{ZnO}] + k_{\mathrm{ZnO-Fe}} \cdot [\mathrm{ZnO}] \qquad [12]$$

Finally, the closed solution of this system of linear differential equations (DSolve method, Mathematica 11; Wolfram Research, IL) is given:

$$\mathrm{FeO}_{(t)} = \frac{e^{-k_{\mathrm{FeO-C}} \cdot t}}{k_{\mathrm{FeO-C}} \cdot (k_{\mathrm{FeO-C}} - k_{\mathrm{ZnO-C}} - k_{\mathrm{ZnO-Fe}})} \cdot \left(k_{\mathrm{FeO-C}} \cdot \left[[\mathrm{FeO}]_0 \cdot (-k_{\mathrm{ZnO-C}} + k_{\mathrm{FeO-C}} - k_{\mathrm{ZnO-Fe}}) - k_{\mathrm{ZnO-Fe}} \cdot [\mathrm{ZnO}]_0 + k_{\mathrm{ZnO-Fe}} \cdot [\mathrm{ZnO}]_0 \cdot e^{t \cdot (k_{\mathrm{FeO-C}} - k_{\mathrm{ZnO-C}} - k_{\mathrm{ZnO-Fe}})} \right. \right. \left. \left. - k_{\mathrm{FeO-Oxi}} \right] + k_{\mathrm{FeO-Oxi}} \cdot \left[k_{\mathrm{ZnO-C}} \left(1 - e^{k_{\mathrm{FeO-C}} \cdot t}\right) + \cdot e^{k_{\mathrm{FeO-C}} \cdot t} (k_{\mathrm{FeO-C}} - k_{\mathrm{ZnO-Fe}}) + k_{\mathrm{ZnO-Fe}} \right] \right) \qquad [\mathrm{I}]$$

$$\mathrm{ZnO}_{(t)} = [\mathrm{ZnO}]_0 \cdot e^{-(k_{\mathrm{ZnO-C}} + k_{\mathrm{ZnO-Fe}}) \cdot t} \qquad [\mathrm{II}]$$

Resulting Eqs. [I] and [II] describe the time-dependent FeO and ZnO concentrations as a function of time, four temperature dependent rate constants ($k_{\mathrm{FeO-C}}, k_{\mathrm{ZnO-C}}, k_{\mathrm{ZnO-Fe}}, k_{\mathrm{FeO-Oxi}}$) and the starting concentrations (FeO_0, ZnO_0) at t = 0. The rate constants for FeO and ZnO can be approximated by the method of least squares to the experimental data. The rate constants are not solely determined by temperature and concentration, but also by the ratio of phase boundary area (= reaction area) to slag mass. In the present study, slag mass losses due to sampling and ongoing reactions are not considered. The assumption of a constant ratio of slag mass to phase boundary area is consequently used to calculate the mass transfer coefficient (MTC) for FeO and ZnO for the reaction mechanisms outlined in Eqs. [1] through [3].

The mass transfer coefficient (MTC) for a reaction mechanism (j) is defined in Eq. [13], where (k_{J}) is the corresponding rate constant, (A) the phase boundary area, (M_j) the molar mass and (m_{slag}) the slag mass:

$$\mathrm{MTC}_j = k_j \cdot \frac{m_{\mathrm{slag}}}{A \cdot M_j} (\mathrm{mol\ s^{-1}\ m^{-}}) \qquad [13]$$

IV. RESULTS

Figure 2 illustrates effective FeO and ZnO concentrations (markers) for six isothermal experiments at increasing temperatures. Nonlinear regression was used to determine best-fit values for the four rate constants of Eq. I + II for each *individual* experiment and corresponding graphs are plotted.

At the beginning of each experiment the FeO concentration increased, pointing towards Fe oxidation (reverse reaction of Eq. [2]) and metallothermic ZnO reduction (Eq. [3]). Following the sharp initial decline of the ZnO concentration in the slag and at consequently lower ZnO compositions the carbothermic FeO reduction became more dominant, which lead to a steady decrease of the FeO concentration for the remaining experiment. Within the recorded experimental duration (minimum 60 minutes) the FeO concentration did not reach a chemical equilibrium, which impacted the precise determination of the Fe oxidation rate constant, $k_{\mathrm{Fe\text{-}Oxi}}$. Visual evaluations of the graphite crucibles after each experiment showed a lower crucible thickness in the metal area, due to dissolution of C in the liquid iron. This indicates that the reduction reaction predominantly occurs between the liquid metal and slag phase, rather than direct contact of graphite and slag. This agrees with unpublished experiments that only contain a molten slag (no metal bath), were the reduction reaction of ZnO was slow.

By means of Arrhenius plots (Figure 3), the determined *individual* rate constants for all isothermal experiments were combined to *generally* valid, temperature dependent rate constants. The Arrhenius fit of the reduction mechanisms ($k_{\text{FeO-C}}$, $k_{\text{ZnO-C}}$ and $k_{\text{ZnO-Fe}}$) demonstrated good correlation, whereas the Fe oxidation ($k_{\text{Fe-Oxi}}$) does not follow the Arrhenius law. The reason are missing equilibrium conditions for the FeO reduction reaction in Figure 2 (the FeO concentration over time has always a significant slope after the last sample). Table II summarizes the found Arrhenius parameters. The activation energies were 285.7 kJ/mol for $k_{\text{ZnO-C}}$, 100.7 kJ/mol for $k_{\text{FeO-C}}$ and 152.7 kJ/mol for $k_{\text{ZnO-Fe}}$. In combination with the preexponential factor, these Arrhenius parameters present a *general* description of the rate constants with respect to the process temperature. Table III compares individual fitted rate constants (individual) with those calculated using the found Arrhenius parameters (general).

A. *Model Accuracy*

Scatter plots were used to correlate effective FeO and ZnO concentrations with values predicted by the developed kinetic model (Eq. I and II) comparing individual and general rate constants. Figures 4(a) and (b) illustrate the measured values against each *individual* isothermal model (Figure 2). The mean and standard deviation of the difference between measured and modeled FeO and ZnO values was 0.00±0.14 wt pct and -0.02±0.33 wt pct, respectively. The deviation of measurements and modelled outcomes of the *generalized* kinetic model (after applying the Arrhenius equation) is depicted in Figures 4(c) and (d). Note, the average deviations for FeO and ZnO in the individual and general case remained roughly unchanged, which indicates the absence of a systematic error. When comparing the individual with the general model, the standard deviation for measured and modelled FeO concentrations was nearly doubled from 0.14 to 0.26 wt pct. In contrast, the ZnO standard deviation remained at a roughly unchanged percentage. Similarly, the coefficient of determination decreases from 0.98 to 0.94 for FeO but stays same for ZnO.

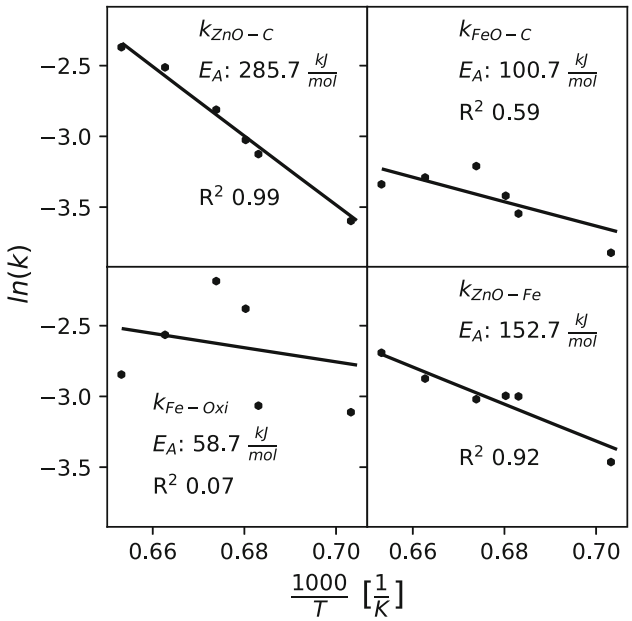

Fig. 3—Arrhenius plots for the rate constants of the kinetic model.

In summary, presented scatter plots demonstrate good correlation between the derived kinetic model and the experimental data. This suggests the suitability of applied approximations (constant slag mass, constant C-concentration in the metal, constant CO partial pressure) and validates the developed kinetic model to describe the reaction mechanism of the high-temperature ZnO and FeO reduction with dissolved C.

B. *Mass Transfer Coefficient*

Finally, the mass transfer coefficient (MTC) for the ZnO reduction mechanisms was derived by recalculating the rate constants according to Eq. [13].

$$\text{MTC}_{\text{ZnO\_C}} = 3.94 \times 10^{8} \cdot e^{\frac{-285.7\,\text{kJ mol}^{-1}}{R \cdot T}}\,\text{mol s}^{-1}\,\text{m}^{-2} \quad [14]$$

$$\text{MTC}_{\text{Zno\_Fe}} = 3.86 \times 10^{4} \cdot e^{\frac{-152.7\,\text{kJ mol}^{-1}}{R \cdot T}}\,\text{mol s}^{-1}\,\text{m}^{-2} \quad [15]$$

Figure 5(a) highlights the threefold increase in overall MTC from 1400 °C to 1500 °C and visualizes the higher temperature dependency of the carbothermic mechanism compared to the metallothermic reaction. With rising temperatures the relative contribution of the carbothermic reaction to the overall reduction increased (Figure 5(b)). While both mechanisms equally influenced the overall reaction below 1400 °C, the carbothermic reaction is dominant at elevated temperatures. The presented methodology is useful to estimate production volumes for given furnace dimensions, dust compositions and process conditions of a recycling treatment applying the iron-bath process.

V. DISCUSSION

Carbothermic reduction is the most successful mechanism to recycle Zn containing industrial wastes, such as EAFD. The widespread use of the Waelz kiln, however, exhibits considerable drawbacks, such as the improvable recovery rate (approx. 85 pct), the generation of Waelz slag and the high specific CO_2 emissions. Donald and Pickles proposed an alternative concept to recycle EAFD with a carbon-saturated iron melt as reduction agent for ZnO,[22] and successfully demonstrated a Zn recovery rate of almost 100 pct. In this study we have presented a mathematical kinetic model which describes the ZnO and FeO reduction with carbon dissolved in an iron melt. Pyro-metallurgical, large-scale lab experiments of a metal bath process to recover Zn from a molten slag phase were performed (1) to accurately describe the fundamental reaction kinetics and (2) to evaluate the contributions of the carbothermic and

Table II. Summary of Determined Arrhenius Parameters for the Defined Reaction Mechanisms

	$k_{ZnO\text{-}C}$	$k_{FeO\text{-}C}$	$k_{Fe\text{-}Oxi}$	$k_{ZnO\text{-}Fe}$
A [min^{-1}]	1.8×10^7	3.3×10^1	4.0·[wt pct min^{-1}]	1.8×10^3
E_a [kJ mol^{-1}]	285.7±19.2	100.7±45.1	58.7±124.9	152.7±23.3

Table III. Summary of Individual and General Rate Constants

	$k_{ZnO\text{-}C}$ [10^{-2} min^{-1}]		$k_{FeO\text{-}C}$ [10^{-2} min^{-1}]		$k_{Fe\text{-}Oxi}$ [10^{-2} wt pct min^{-1}]		$k_{ZnO\text{-}Fe}$ [10^{-2} min^{-1}]	
Temperature (K)	Individual	General	Individual	General	Individual	General	Individual	General
1695	2.7	2.8	2.2	2.6	4.5	6.3	3.1	3.5
1737	4.4	4.6	2.9	3.1	4.7	6.9	5.0	4.5
1743	4.9	5.0	3.3	3.1	9.3	7.0	5.0	4.7
1757	6.0	5.8	4.0	3.3	11.2	7.2	4.9	5.1
1782	8.1	7.6	3.7	3.6	7.7	7.7	5.7	5.9
1804	9.3	9.7	3.6	4.0	5.8	8.0	6.8	6.7
R^2	0.99		0.59		0.07		0.92	

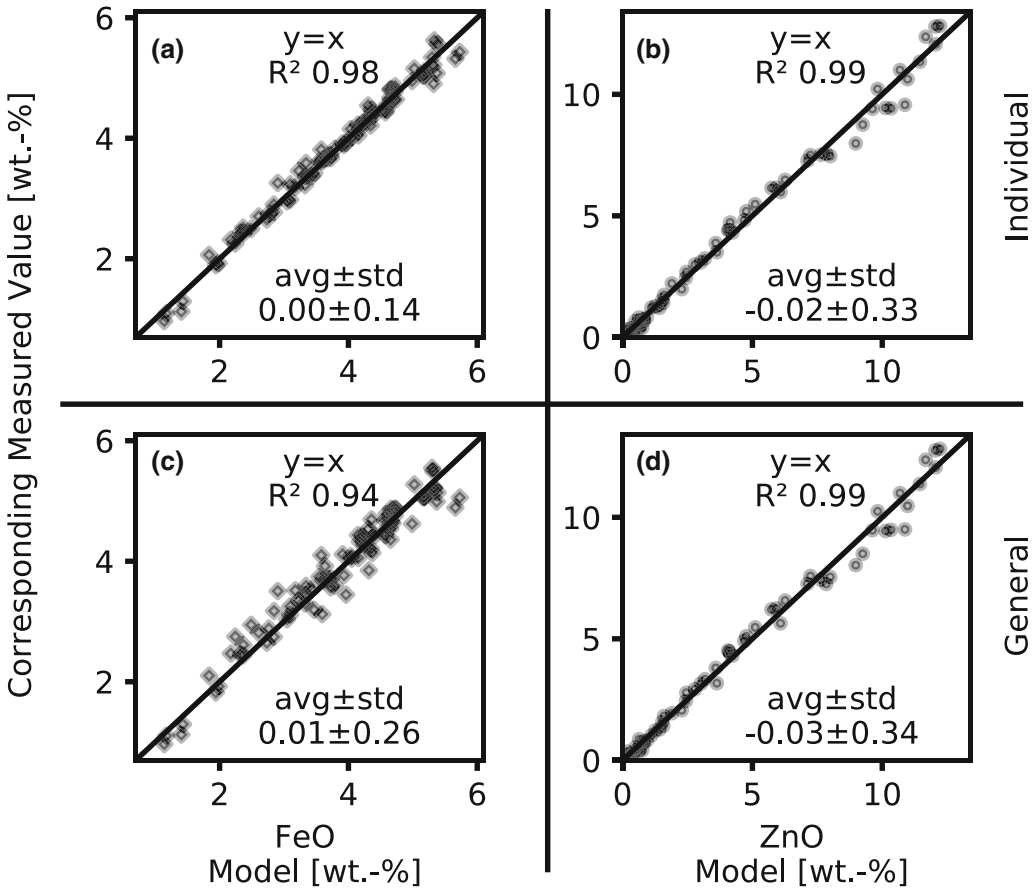

Fig. 4—Scatter plot of the measured effective FeO and ZnO concentrations *vs* calculated model values. The first row shows the deviation between measured and model values for the individual fits (individual) and the second row after applying the Arrhenius correlation to the rate constants (general) (*a*) FeO individual fits, (*b*) ZnO individual fits, (*c*) FeO general fit, (*d*) ZnO general fit.

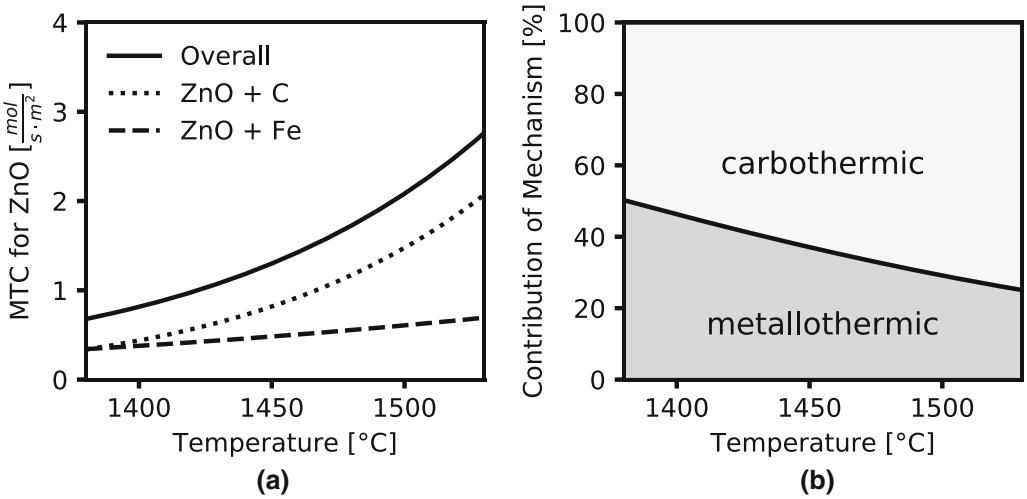

Fig. 5—(*a*) MTC for ZnO depending on the process temperature. (*b*) Share of reaction mechanism for ZnO reduction.

metallothermic reactions. We provide temperature dependent mass transfer coefficients which generally define the reactions of the ZnO and FeO reduction.

The applied mathematical model describing the reaction kinetics of a system of reduction reactions is based on a more simple approach described by Leuchtenmueller *et al.* on the carbothermic chromium oxide reduction.[50] In this study, obtained data of six individual high-temperature reduction experiments were in good agreement (min. $R^2 = 0.94$) with the developed kinetic model. The rate constant of the FeO reverse reaction did not follow the Arrhenius correlation, resulting in more deviation (Figure 4) from the predicted model than the other reactions. This difference was founded in the missing FeO chemical equilibrium in the slag. However, this does not affect the significance of the ZnO reduction. Presented kinetic model resulted in the following main findings:

1. We confirm the reported qualitative observations of Donald and Pickles [22] that carbon-saturated molten iron is an effective method to reduce zinc oxide from a molten slag phase. The ZnO concentrations in the final slag samples were below 0.1 wt pct resulting in Zn recovery rates higher than 99.9 pct. FeO reduction rates of the metal-bath process were comparatively slow.
2. The developed kinetic model applied to the metal-bath process proves that the metallothermic ZnO reduction with Fe is a major contributor to the overall reaction mechanism. Therefore, our experimentally validated model demonstrates that the ZnO reduction is a combination of simultaneous carbothermic and metallothermic reactions. The model establishes that two reduction reactions of metal oxides in slags can occur simultaneously (given sufficient thermodynamic driving force), which directly contradicts previous reports, which state that FeO will be reduced prior to ZnO.[51]

Furthermore, when considering the reduction of ZnO in contact with a C-saturated liquid Fe melt based solely on thermodynamics, the assumption may prevail that the more noble (less oxygen affine) Fe does not participate in the reduction reaction. Yet, this study confirms a significant contribution of Fe to the overall ZnO reduction.

3. This study applied the combination of a mathematically derived kinetic model verified by experiments to provide quantitative information on the ZnO reduction mechanism.

The carbothermic reaction exhibited a significantly higher temperature dependency than the metallothermic reaction, which reduced the contribution of the metallothermic reduction to the overall reaction from approximately 50 pct at 1400 °C to 25 pct at 1500 °C. Such a temperature rise (from 1400 °C to 1500 °C) also increased the total mass transfer of the zinc oxide reduction from approximately 0.7 to ~ 2.8 [mol s^{-1} m^{-2}].

The presented experimental data does not allow the precise determination of the rate limiting step. However, the authors propose that the formation of gaseous zinc at the metal-slag boundary could be limiting the reaction speed. The availability of a carrier gas is assumed to increase the ZnO reduction. Kim *et al.* describe in a similar setting improved ZnO reduction rates at higher FeO concentrations and proposed a reaction between ZnO and FeO to form Zn and Fe_2O_3.[48,49] However, we believe that the elevated kinetics reported by Kim *et al.* may have been a result of the increased CO formation, which increased the Zn gas development.

Zn containing waste materials, such as EAFD, can contain up to 0.5 pct Cu. During the metal bath process Cu would accumulate in the Fe-rich metallic phase and produce Cu-contaminated pig iron as by-product. To achieve economic operations the metal bath process should avoid excessive FeO reduction and produce a

FeO-rich slag without volatiles (Zn, Pb, Cl) and impurities (Cu) which could be recycled in integrated steel mills.

The experimental setup and established model were able to mimic certain aspects of the recycling of zinc-containing industrial wastes, but presented results must be viewed considering following limitations: (1) Only one defined slag composition was investigated; (2) A synthetic slag was used to model an industrial waste composition; (3) A constant slag mass, (4) constant C-concentration in the metal and (5) constant CO partial pressure were assumed to simplify the mathematical model; (6) Given temperature fluctuations occurred. Future work should focus on these limitations and include the kinetic influence of the slag FeO concentration.

VI. CONCLUSION

Our mathematical kinetic model is the first study to fundamentally describe the combined kinetics of three simultaneously occurring reactions of the carbothermic ZnO reduction with liquid, molten phases including the reduction agents, carbon and iron. We conclude that carbothermic and metallothermic reactions occur simultaneously, and that the metallothermic reduction is a major contributing process tipping the balance towards a more pronounced ZnO reduction. The presented kinetic model may be used to design a recycling treatment for zinc-containing industrial wastes applying a carbon-saturated iron-bath process.

ACKNOWLEDGMENT

This work was supported by the Austrian Research Promotion Agency (FFG).

FUNDING

Open access funding provided by Montanuniversität Leoben.

REFERENCES

1. S. Spatari, M. Bertram, K. Fuse, T.E. Graedel, and E. Shelov: *Resour. Conserv. Recycl.*, 2003, vol. 39, pp. 137–60.
2. S.R. Taylor: *Geochim. Cosmochim. Acta*, 1964, vol. 28, pp. 1273–85.
3. H.-W. Ma, K. Matsubae, K. Nakajima, M.-S. Tsai, K.-H. Shao, P.-C. Chen, C.-H. Lee, and T. Nagasaka: *Resour. Conserv. Recycl.*, 2011, vol. 56, pp. 134–40.
4. G. Meylan and B.K. Reck: *Resour. Conserv. Recycl.*, 2017, vol. 123, pp. 1–10.
5. M.K. Jha, V. Kumar, and R.J. Singh: *Resour. Conserv. Recycl.*, 2001, vol. 33, pp. 1–22.
6. R.L. Nyirenda: *Min. Eng.*, 1991, vol. 4, pp. 1003–25.
7. X. Lin, Z. Peng, J. Yan, Z. Li, J.-Y. Hwang, Y. Zhang, G. Li, and T. Jiang: *J. Clean. Prod.*, 2017, vol. 149, pp. 1079–1100.
8. L.R.P.D.A. Lima and L.A. Bernardez: *J. Hazard. Mater.*, 2011, vol. 189, pp. 692–99.
9. B.-S. Kim, S.-B. Jeong, J.-C. Lee, D. Shin, and N.-I. Moon: *Mater. Trans.*, 2012, vol. 53, pp. 985–90.
10. A.L. Riley, S.E. Pepper, A.J. Canner, S.F. Brown, and M.D. Ogden: *Separ. Sci. Technol.*, 2018, vol. 53, pp. 22–35.
11. R. Remus, M. A. Monsonet, S. Roudier, and L. D. Sancho: *Luxembourg: Publications Office of the European Union*, 2013, p. 621.
12. A.-G. Guézennec, J.-C. Huber, F. Patisson, P. Sessiecq, J.-P. Birat, and D. Ablitzer: *Powder Technol.*, 2005, vol. 157, pp. 2–11.
13. World Steel in Figures 2019.
14. J.G.M.S. Machado, F.A. Brehm, C.A.M. Moraes, C.A.D. Santos, A.C.F. Vilela, and J.B.M.D. Cunha: *J. Hazard. Mater.*, 2006, vol. 136, pp. 953–60.
15. C.A. Pickles: *Min. Process. Extract. Metall.*, 2003, vol. 112, pp. 81–89.
16. J.C. Wang, M.T. Hepworth, and K.J. Reid: *JOM*, 1990, vol. 42, pp. 42–45.
17. T. Suetens, B. Klaasen, K. van Acker, and B. Blanpain: *J. Clean. Product.*, 2014, vol. 65, pp. 152–67.
18. J. Antrekowitsch, G. Rösler, and S. Steinacker: *Chem. Ingen. Tech.*, 2015, vol. 87, pp. 1498–1503.
19. S. Pauliuk, R.L. Milford, D.B. Müller, and J.M. Allwood: *Environ. Sci. Technol.*, 2013, vol. 47, pp. 3448–54.
20. M. Atkinson and R. Kolarik: Steel Industry Technology Roadmap, 2001.
21. B. Cubukcuoglu and S. Ouki: *The Use of Alternative Constituents in Cement-Based Solidification/Stabilisation of Electric Arc Furnace Dust*, 2009.
22. J.R. Donald and C.A. Pickles: *Can. Metall. Q.*, 1996, vol. 35, pp. 255–67.
23. O.D.A. Hiroshi, T. Ibaraki, and Y. Abe: *Nippon Steel Technical Report No. 94*, 2006.
24. K. Mager, U. Meurer, B. Garcia-Egocheaga, N. Goicoechea, J. Rutten, W. Saage, and F. Simonetti: *Recycling of Metals and Engineercd Materials*, Ed. by D. L. Stewart, J. C. Daley, and R. L. Stephens, Wiley, Hoboken, NJ, 2000, pp. 329–44.
25. M. Nakayama: *SEAISI Q.*, 2012, vol. 41, pp. 22–26.
26. E.C. Schoukens, S. Afs *et al.*: *J. South. Afr. Inst. Min. Metall.*, 1993, vol. 93, pp. 1–7.
27. M.G. Maccagni: *J. Sustain. Metall.*, 2016, vol. 2, pp. 133–40.
28. J.A. Asteljoki, *Method for Producing Zinc by Means of Iron Melt Reduction*, 0 433 674 A1.
29. I. Vegas, J.A. Ibañez, J.T. San-José, and A. Urzelai: *Waste Manag.*, 2008, vol. 28, pp. 565–74.

30. H. Maczek and R. Kola: *JOM*, 1980, vol. 32, pp. 53–58.
31. P.I. Grudinsky, D.V. Zinoveev, V.G. Dyubanov, and P.A. Kozlov: *Inorg. Mater. Appl. Res.*, 2019, vol. 10, pp. 1220–26.
32. V.I. Matyukhin, O.V. Matyukhin, V.V. Shatsillo, A.V. Matyukhina, and O.S. Koshcheeva: *Metallurgist*, 2017, vol. 60, pp. 1025–31.
33. S. Sorlini, C. Collivignarelli, G. Plizzari, and M. D. Foglie: In: *Proceedings of the "International RILEM Conference on the use of recycled materials in buildings and structures",* RILEM publications, Barcelona, 2004, pp. 9–11.
34. G.-S. Lee and Y.J. Song: *Min. Eng.*, 2007, vol. 20, pp. 739–46.
35. O. Ruiz, C. Clemente, M. Alonso, and F.J. Alguacil: *J. Hazard. Mater.*, 2007, vol. 141, pp. 33–36.
36. P. Palimąka, S. Pietrzyk, M. Stępień, K. Ciećko, and I. Nejman: *Metals*, 2018, vol. 8, p. 547.
37. C. Lanzerstorfer: *J. Clean. Product.*, 2018, vol. 174, pp. 1–6.
38. S. Itoh, A. Tsubone, K. Matsubae-Yokoyama, K. Nakajima, and T. Nagasaka: *ISIJ Int.*, 2008, vol. 48, pp. 1339–44.
39. R. Chairaksa-Fujimoto, Y. Inoue, N. Umeda, S. Itoh, and T. Nagasaka: *Int. J. Miner. Metall. Mater.*, 2015, vol. 22, pp. 788–97.
40. R. Chairaksa-Fujimoto, K. Maruyama, T. Miki, and T. Nagasaka: *Hydrometallurgy*, 2016, vol. 159, pp. 120–25.
41. T. Sofilić, A. Rastovcan-Mioc, S. Cerjan-Stefanović, V. Novosel-Radović, and M. Jenko: *J. Hazard. Mater.*, 2004, vol. 109, pp. 59–70.
42. M.C. Mantovani, C. Takano, and P.M. Büchler: *Ironmak. & Steelmak.*, 2004, vol. 31, pp. 325–32.
43. Y. Li, Z. Liu, H. Liu, and B. Peng: *J. Clean. Prod.*, 2017, vol. 143, pp. 311–18.
44. W.J. Rankin and S. Wright: *Metall. Mater. Trans. B*, 1990, vol. 21, pp. 885–97.
45. H.-K. Chen: *Scand. J. Metall.*, 2001, vol. 30, pp. 292–96.
46. B.-S. Kim, J.-M. Yoo, J.-T. Park, and J.-C. Lee: *Mater. Trans.*, 2006, vol. 47, pp. 2421–26.
47. Y. Kuwauchi and M. Barati: *ISIJ Int.*, 2013, vol. 53, pp. 1097–105.
48. J.R. Donald and C.A. Pickles: *Metall. Mater. Trans. B*, 1996, vol. 27, pp. 363–74.
49. M. Leuchtenmueller, W. Schatzmann, and S. Steinlechner: *J. Environ. Chem. Eng.*, 2020, vol. 8, p. 103976.
50. M. Leuchtenmüller, J. Antrekowitsch, and S. Steinlechner: *Metall. Mater. Trans. B*, 2019, vol. 50, pp. 2221–28.
51. P.A. Kozlov: *The Waelz Process,* Ore and Metals Publishing House, 2003.